Turkish Journal of Earth Sciences

Volume 33
Number 1 *SI-1*

Article 7

1-4-2024

Soil liquefaction and subsidence disaster in İskenderun related to the 6 February 2023 Pazarcık (Mw: 7.7) and 20 February Defne (Mw: 6.4) earthquakes, Türkiye

HÜSEYİN ÖZTÜRK
ozturkh@istanbul.edu.tr

CRAIG A. DAVIS

İBRAHİM KUŞKU

SÜLEYMAN DALĞIÇ
dalgic@istanbul.edu.tr

CEM KASAPÇI

See next page for additional authors

Soil liquefaction and subsidence disaster in İskenderun related to the 6 February 2023 Pazarcık (Mw: 7.7) and 20 February Defne (Mw: 6.4) earthquakes, Türkiye

Authors
HÜSEYİN ÖZTÜRK, CRAIG A. DAVIS, İBRAHİM KUŞKU, SÜLEYMAN DALĞIÇ, CEM KASAPÇI, and MUHARREM ALPER ŞENGÜL

TÜBİTAK

Turkish Journal of Earth Sciences

http://journals.tubitak.gov.tr/earth/

Research Article

Turkish J Earth Sci
(2024) 33: 85-98

doi:10.55730/1300-0985.1900

Soil liquefaction and subsidence disaster in İskenderun related to the 6 February 2023 Pazarcık (Mw: 7.7) and 20 February Defne (Mw: 6.4) earthquakes, Türkiye

Hüseyin ÖZTÜRK[1,*], Craig A. DAVIS[2], İbrahim KUŞKU[1], Süleyman DALĞIÇ[1], Cem KASAPÇI[1], Muharrem Alper ŞENGÜL[3]

[1]Department of Geological Engineering, Faculty of Engineering, İstanbul University-Cerrahpaşa, İstanbul, Turkiye
[2]Los Angeles Department of Water and Power, Los Angeles, USA
[3]Institute of Graduate Studies, İstanbul University-Cerrahpaşa, İstanbul, Turkiye

Received: 06.06.2023 • **Accepted/Published Online:** 07.11.2023 • **Final Version:** 04.01.2024

Abstract: The Mw 7.7 Pazarcık earthquake on February 06, 2023, struck southern Türkiye, causing typical liquefaction along the shores of İskenderun Bay. This liquefaction was characterized by lateral spreading, subsidence, and flooding. Subsidence-triggered sand ejecta, water flows, and opening cracks were identified in areas spanning approximately 2 km in length and 300 m in width.

Based on coastal references such as lighthouses or harbor platforms, settlements of 0.8 m and lateral spreading of 0.4% were recorded along the coastal zone following the Pazarcık earthquake. According to camera recordings, liquefaction-related water and silty sand outflows occurred 29 min after the earthquake. The largest water outlet observed had dimensions of 2 m in length, 1 m in width, and 0.5 m in depth. Images captured at the moment of liquefaction show water gushing for 2 m.

Granulometric analysis of liquefied sand eruptions at 10 locations on the coast of İskenderun indicated the presence of silty sand (SM). No water entered the settlement area from the sea during or shortly after the earthquake. The waters that flooded the streets of İskenderun were largely drained or pumped out after remaining for 3 days. The liquefaction of the main soil zone played a crucial role in the collapse or tilting of tall buildings along the shores of İskenderun.Lateral spreading and collapse on the shores of İskenderun were further exacerbated by the MW 6.4 magnitude Defne earthquake that occurred 14 days after the initial major earthquake. Field observations made 25 days after the first earthquake revealed a settlement of 1.7 m and approximately 1% lateral spreading in the coastal zone of İskenderun.

Key words: Earthquake, liquefaction, subsidence, lateral spreading, flooding, Türkiye

1. Introduction

On February 6, 2023, two strong earthquakes with moment magnitudes Mw 7.7 and Mw 7.6 struck in Türkiye, as indicated in Figure 1. The Mw 7.7 Pazarcık earthquake occurred at 04:17 local time on the Eastern Anatolian Fault (EAF) system, while the Mw 7.6 Elbistan earthquake struck at 13:24 Turkish time on the Çardak Fault System. The EAF ruptured bilaterally from the epicenter inland towards the northeast and southwesterly towards the Mediterranean coast, with an approximate total rupture length of 350 km (AFAD, 2023; Goldberg et al., 2023). İskenderun city, located about 20 km from the surface rupture, was heavily impacted by the earthquake. Significant building damages, particularly in the coastal zone, resulted in numerous casualties. The earthquake led to the formation of a curious pool of water up to 30 cm deep on the coastal roads and streets, which the media presented as being flooded due to seawater occupation[1]. This flooding occurred in areas such as Atatürk Boulevard, Mete Aslan Street, and Atatürk Monument. The focus of this paper is on the investigation of this flooding zone.

Postearthquake site investigations revealed evidence of liquefaction along the coast, especially within the flooded zone. Liquefaction induces three main mechanisms of permanent ground deformations, defined as (1) ejecta-induced ground deformation, (2) volumetric-induced ground deformation, and (3) shear-induced ground deformation (Bray and Macedo, 2017; Quintero et al. 2018). As detailed in this paper, these three ground deformation mechanisms are hypothesized to have played crucial roles in the observed postearthquake flooding. Liquefaction phenomena are often associated with the ejection of water

1 Aykırı (2006). İskenderun sular altında! Deprem sonrası bir anda yükseldi [online]. Website https://www.aykiri.com.tr/İskenderun-sular-altinda-deprem-sonrasi-bir-anda-yukseldi/34135 [accessed 10 February 2023] (in Turkish).

* Correspondence: ozturkh@iuc.edu.tr

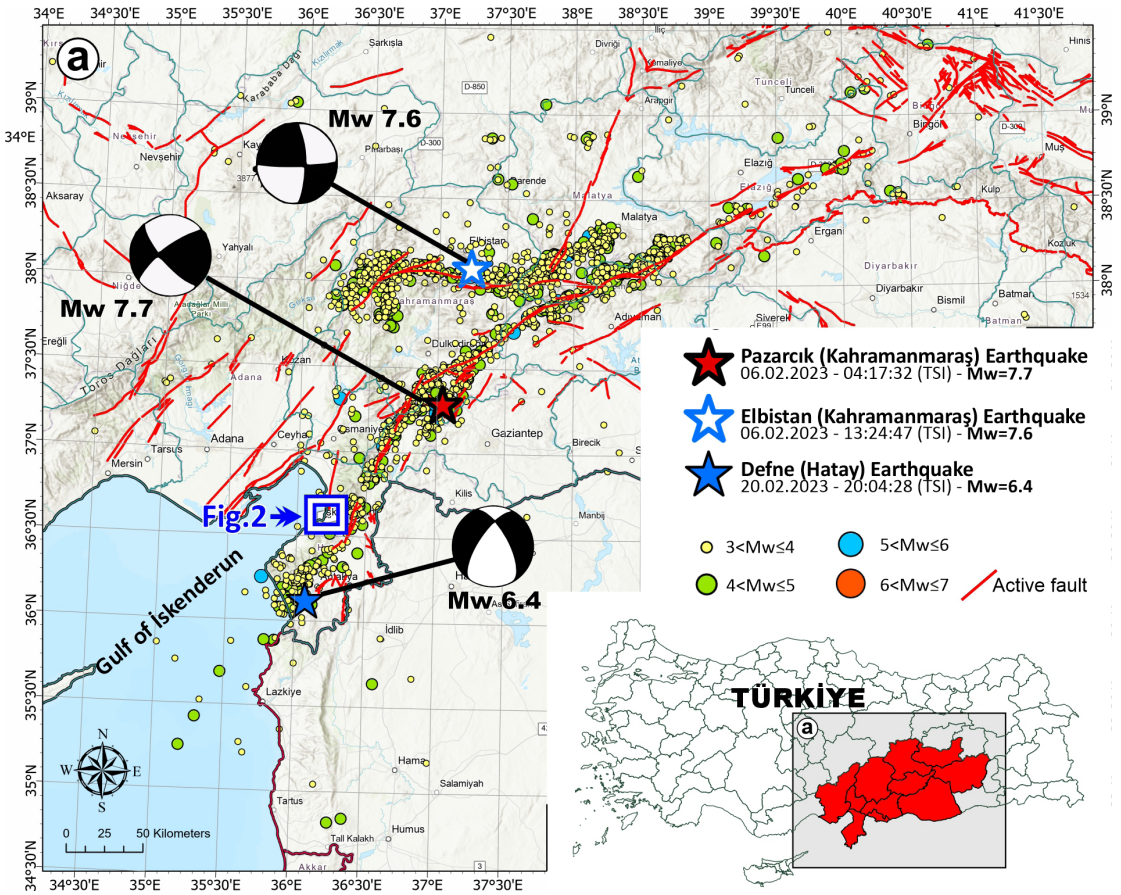

Figure 1. The epicenters of the Pazarcık Mw: 7.7 and Elbistan Mw: 7.6 earthquakes that occurred on February 6, 2023, and the Defne Mw: 6.4 earthquake that occurred on February 20, 2023 (AFAD, 2023). The blue square shows the location of the study area.

and sand onto the ground surface (Seed and Idriss, 1971; Ishihara and Yoshimine, 1992; Andrus et al., 2001; Youe et al., 2001; Seed et al., 2003; Dixon et al., 2006; Measures et al., 2011; Galavi et al., 2013; Quigley et al., 2013; Green et al., 2014). The resulting sand deposits are referred to as sand boils. Numerous studies describe the occurrence of water and sand boiling associated with soil liquefaction following earthquakes worldwide. Examples include the 2010–2011 Canterbury Earthquake Sequence (CES) in Christchurch, New Zealand (Giovinazzi et al., 2011; Villamor et al., 2016), the 1995 Hyogoken–Nambu earthquake in Kobe, Japan, and around Osaka Bay (Tanaka, 1996; Mase et al., 2022), the 1963 Gulf of Alaska earthquake (Lemke, 1967), and the 2018 Indonesia earthquake (Hidayat et al., 2020). One of the most notable and disruptive impacts of soil liquefaction was the inundation of coastal settlements by water and sand, associated with the discharge of groundwater onto the ground surface after various events in the 2010–2011 CES (Davis et al., 2015; Villamor et al., 2016).

Land surveys were conducted between February 11 and 12, shortly after the earthquake on February 6, 2023, in the coastal zones of İskenderun to determine the source of the water that flooded the streets before any traces of the earthquake were erased. During this period, all opening cracks and sand boil locations were marked on the Google Earth map, and samples of the sand forming the boils were collected for later granulometric tests. Fourteen days after the initial earthquake, the Mw 6.4 Defne earthquake impacted the İskenderun region, further accelerating coastal subsidence and leading to seawater occupation for the first time. Due to the subsequent influx of water into the streets, the region was revisited on March 13, 2023, to observe the widening of ground cracks and increased subsidence at the previously measured fixed points.

2. Geology and soil structure of the İskenderun coastal zone

Figure 2 presents the geological map and a cross-section of the coastal zone. In Figure 2a, the geology of the

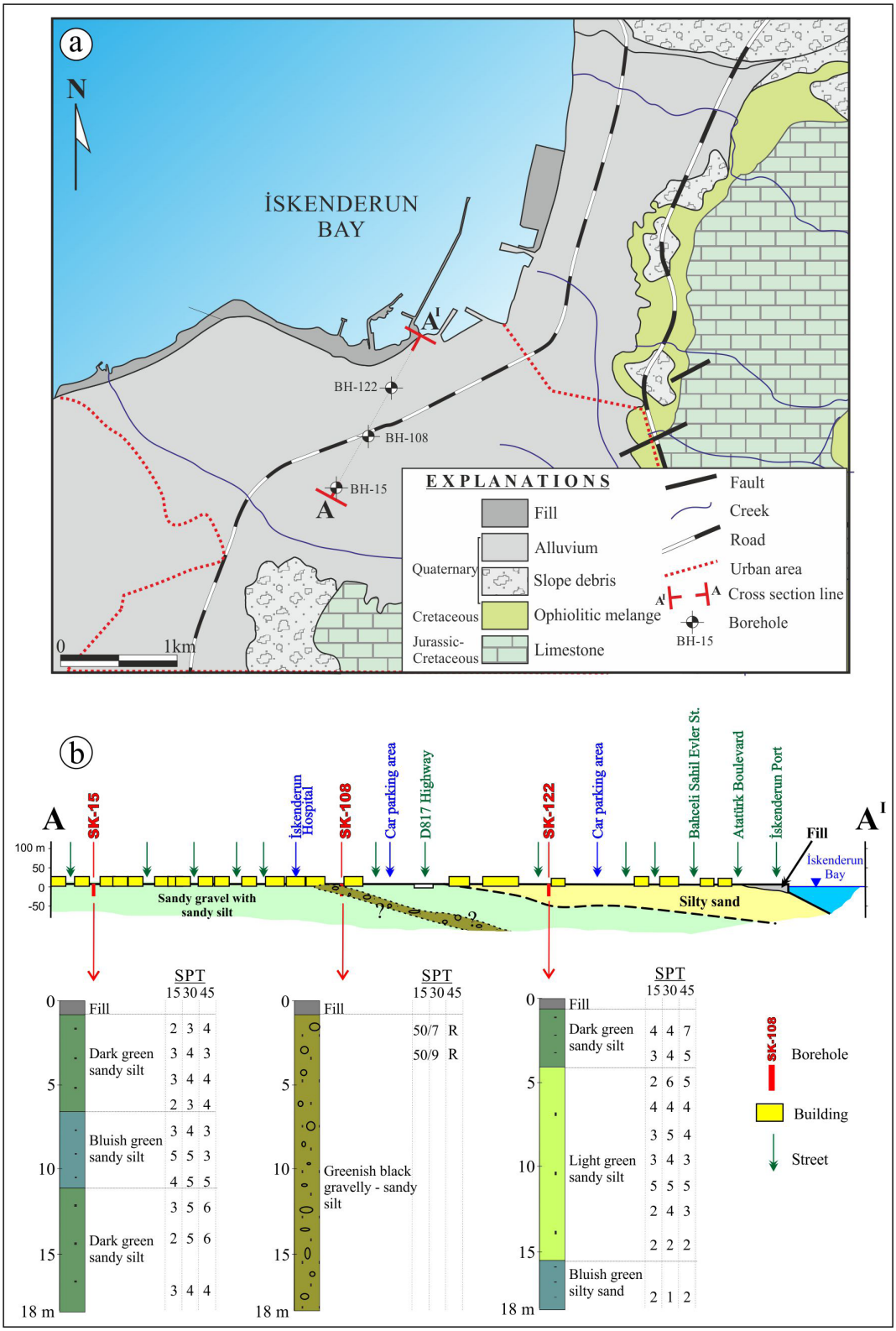

Figure 2. a) Geological map of the İskenderun coast depicting alluvial plains, creeks flowing into the sea and the areas filled in after 1970. The filled coastal zone materials are approximated on the geological map. b) Correlation of the geotechnical borehole logs along section A-A', as shown in Figure 2a, illustrating weak alluvial soil conditions characterized by low SPT values.

İskenderun Bay coastal zone is depicted, comprising serpentinite and limestone from the Mesozoic era, as well as quaternary alluvium and colluvial fan. While the Mineral Research and Exploration General Directorate of Türkiye has designated an active fault segment to the north of İskenderun that extends into the region, no active fault has been detected within İskenderun Bay itself. Öztürk et al. (2021) have proposed the presence of low-angle normal faults that influenced the post-Pliocene uplifting of the Amanos Mountain and the formation of the flat coastal plain. The İskenderun Bay is situated 20 km west of the fault segment associated with the main event. Figure 1 displays numerous aftershocks near the İskenderun shore, which may be linked to blind normal faults.

Soil investigations in İskenderun were conducted by Denge Engineering Company (Denge, 2010), revealing through geotechnical tests and geological-geophysical studies that the alluvial soils have the potential to liquefy. Figure 2b illustrates the presence of very weak alluvial soil conditions, characterized by very low N30 standard penetration test blow count values ranging from 3 to 11 down to a depth of 18 m in three bore holes. Deeper borehole investigations have also indicated the presence of sandy gravel layers up to 40 m thick in the silty sand sediment (Denge, 2010). The İskenderun coastal plain has a shallow groundwater table, located 1–3 m below the ground surface, depending on the distance from the seashore. High-rise building structures were constructed on these weak soil conditions along the coast. In addition to the water-saturated alluvium, an artificial fill, approximately 200 to 300 m wide and 2 km long, was placed along the coastal zone. This artificial fill was deposited between the years 1960 and 2000, and areas reclaimed from the sea were utilized for parks, sports facilities, and walking paths. Furthermore, the boring logs shown in Figure 2a indicate a thin layer of fill placed over most of the study area.

3. Coastal zone findings

Figure 3 displays a satellite image of the study area, indicating the locations of tension cracks, the boundary of observed lateral spreading, the area of surface flooding, and locations of photographs, a video, and sand ejecta sampling. Following the Pazarcık earthquake, it was observed that the artificial fill settled and spread laterally. Liquefaction-induced sandy water jets were ejected onto the ground surface, which then collected and flooded the streets in the areas shown in Figure 3. In Figures 4a and 4b, images depict water inundating the streets after the 06 February earthquakes, a situation described by the national media as being associated with seawater inundation, without any coastal observation. Site investigations identified the silty sand boils that were ejected during the

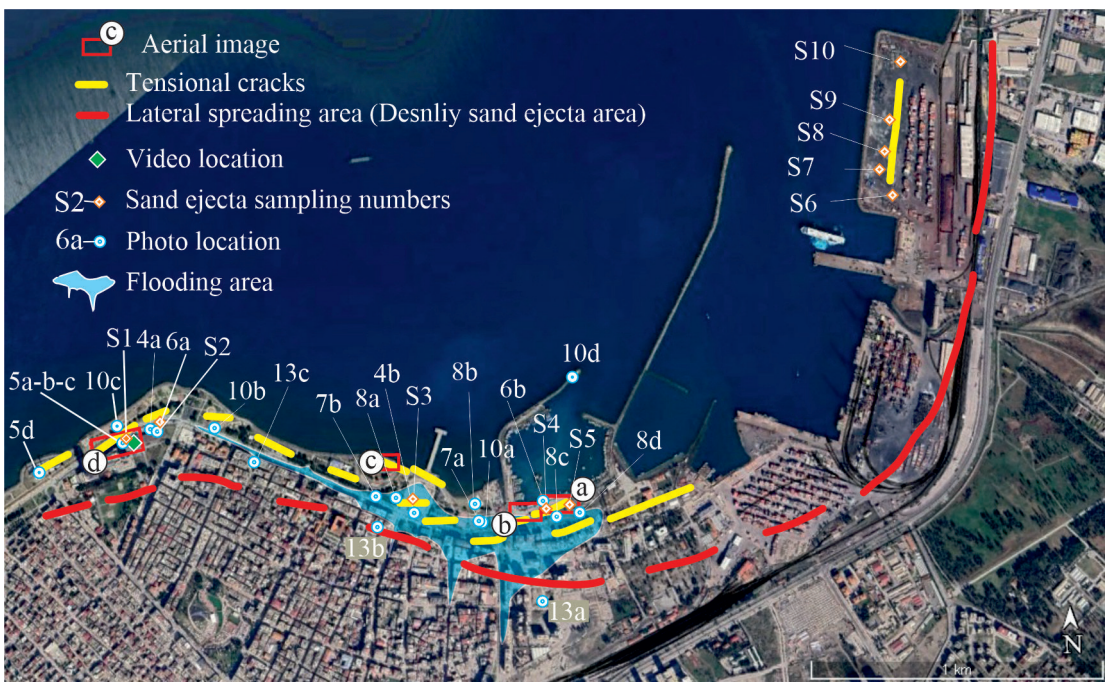

Figure 3. Map showing flooded areas following the Mw: 7.7 Pazarcık earthquake, featuring opening cracks (in yellow), zones of pronounced liquefaction and lateral spreading (highlighted by red lines), sampling sites for sand ejecta, locations of the photographs and video records utilized in Figures 4 to 8, and locations of aerial photos in Figures 9a to 9d.

Figure 4. Water inundating the streets along the İskenderun coast following the February 6, 2023, Pazarcık earthquake. Figure 4a is an aerial photo taken facing southeast from the position marked in Figure 3. Figure 4b is an aerial photo taken facing northwest from the location indicated in Figure 3[1].

1 Hürriyet (2023). Hatay İskenderun'da deniz seviyesi yükseldi [online]. Website https://www.hurriyet.com.tr/gundem/hatay-İskenderunda-deniz-seviyesi-yukseldi-42216512 (in Turkish).

liquefaction process and left behind from the waters gushing from cracks in the fill and alluvium. Figure 5 displays photographs and a still shot image taken from a recorded video from a security camera at a military building. The location of these images can be found with the identification numbers 5a to 5d in Figure 3. Upon examination of the video record obtained from the military building, water and soil are observed gushing out of the ground at a height of about 2 m at 29 min after the earthquake[2]. The field investigation identified this as emerging through an elliptical slit formed naturally in the ground, with a length of 2 m and a width of 1 m. At least 80 m^3 of silty sand material from the natural ground is estimated to have been ejected, based on a measured 20 m × 20 m × 0.2 m volume of soil remaining behind this liquefaction water outlet. Figure 5d is taken at the Nihal Atakaş Mosque and corresponds to the same number in Figure 3. This location also experienced liquefaction and silty water outflow in the courtyard of the Nihal Atakaş Mosque located on the coastline; here, about 45 m^3 of sand remained on the ground surface, with dimensions of 15 m × 20 m × 0.15 m.

Silty water emerges from cracks along the entire filled area along the coastline, with sandy silt accumulating in the form of volcanic cones at the edges of these cracks. Liquefied sandy silt was sampled from these two points. The nature of the particle size fractions of the samples is provided under the liquefaction heading. Figures 6a–6d show sand boils from liquefaction that developed within the artificial fill placed along the coastal zone in grassy areas along the beach. Ejecta was also observed at the base of the electricity poles and along the outer edges of the subsided buildings. Figure 7 demonstrates how fine-grained greenish-black silty sand was discharged onto the ground surface, not only from the cracks in the fill (Figure 7a) but also from around the sewer manholes (Figure 7b). Field observations indicate that a significant amount of water flowed to the surface from around the manholes. The relative movement between the manhole and the paved street resulted in the breaking of the pavement. This could have occurred from uplift of the sewer from pressure coming from the bottom of the sewer manholes and/or settlement of the ground around the manhole.

To investigate the media report suggesting that the flooding shown in Figure 4 was from the sea, no sand or living remains related to the sea were found on and between the rock blocks laid on the coastal belt. This clearly shows that no water came to the roads from the sea. There was also no evidence of an influx of seawater anywhere along the grassy areas located along the shoreline. Figures 7 and 8 provide visual evidence of this observation. Figures 9a–9d plot lateral spreading cracks and sand cones associated with the main earthquake. Figure 9 plots are using Google Earth views. It is noteworthy that taller buildings settled much more than shorter ones. For instance, some small buildings remained at a relatively higher position.

4. Granulometric analysis of the liquefied sediments

Sieve analysis and hydrometer tests were conducted in accordance with the TS EN ISO 17892-4 standard to assess liquefaction. This evaluation was based on 10 samples of fine-grained sand ejecta collected from various locations in the study area, as indicated in Figure 3. The particle size distributions were utilized to gauge the potential for these soils to undergo liquefaction. The graph in Figure 10 (Das, 1983) illustrates the grain size distributions. Grain size analyses revealed that the sand ejecta predominantly consisted of fine-grained sand, with smaller proportions of silt and clay. Among the 10 granulometry analyses per-

2 The video can be accessed on Google Drive: https://drive.google.com/file/d/1pi7bREU1DvuzL3vIyPQv2xAJGVG2A3vs/view?usp=sharing

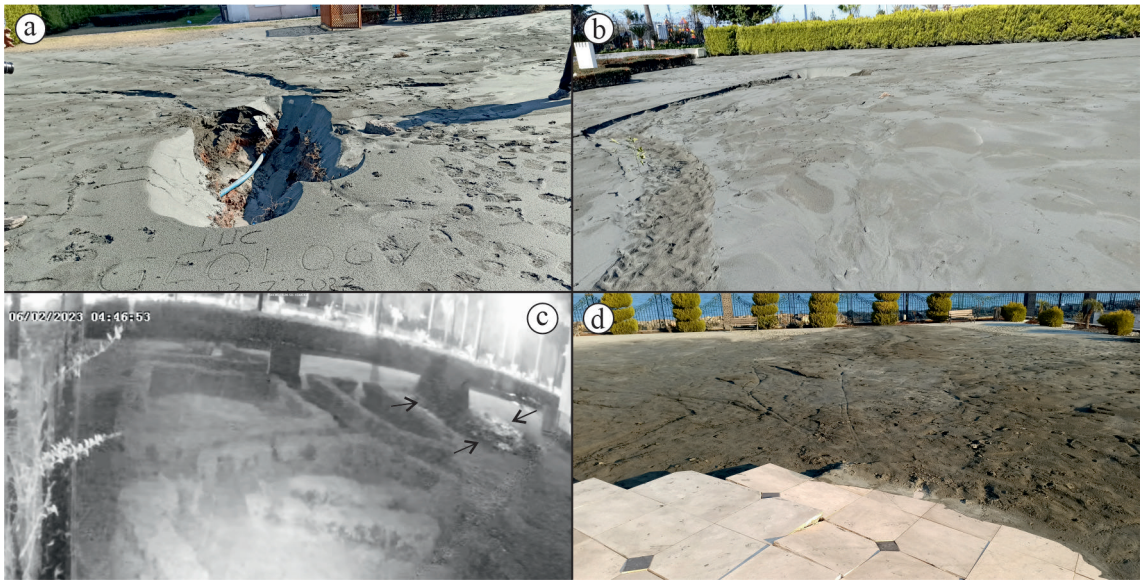

Figure 5. a) Field photograph of the spray point. b) Field photograph of the accumulation area of water and sand spray in the garden of the military building on the coast of İskenderun. c) Still image from the video recording capturing the water tap incident that took place 29 min after the earthquake. d) Sand residue observed in the garden of Nihal Atakaş Mosque.

Figure 6. Silty sand cones formed in parks, at the base of poles, and around foundations along the shoreline. These resulted from water-soil slurry ejected from the ground due to liquefaction. İmage locations are indicated in Figure 3.

formed, it was observed that 8 samples fell within the liquefiable range, while the remaining 2 samples, containing higher levels of clay and silt (S10 and S6), were outside this range (Figure 10). Similar soils, characterized by clayey silt fractions, were reported by Arel and Önalp (2012) to have caused liquefaction-related settlements in the 1999 Adapazarı earthquake in Türkiye, akin to the liquefaction observed in İskenderun.

5. 20 February Defne-Hatay earthquake (Mw: 6.4) and its effects on the İskenderun coasts

Fourteen days after the earthquake on February 6, 2023, another aftershock occurred on February 20, 2023, with a magnitude of Mw 6.4. The epicenter of this event is shown in Figure 1. Photographs in Figures 11a–11c document the effects of this aftershock. It intensified lateral spreading and settlement along the coasts of İskenderun. The

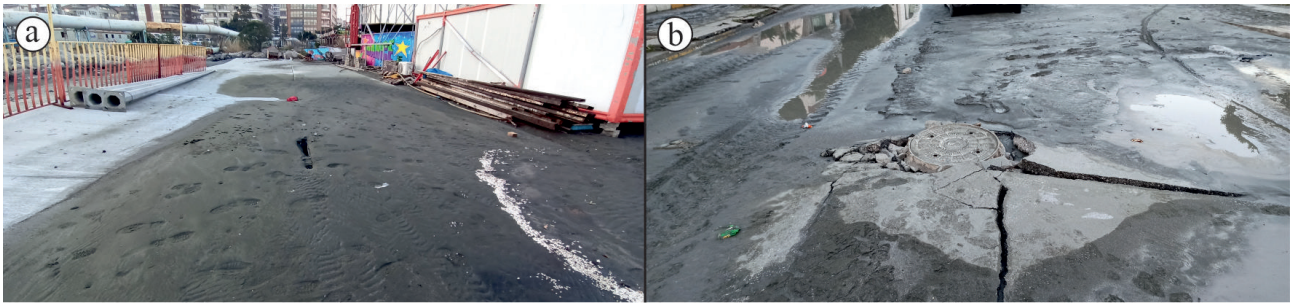

Figure 7. a) Sand emerging from the crack in the amusement park area. b) Sewage water collection structures have risen on the main street due to subsidence of soft sediments. Image locations are indicated in Figure 3.

Figure 8. a) Local puddle and liquefaction-related silt heaps on the road 6 days after the earthquake. b) Cracking in the fishery port due to the splitting and settlement of the coastal fill. Standing greens indicate that seawater has not come from the sea to the shore. Image locations are indicated in Figure 3.

settlement was so extensive that the 1.7-m-high lighthouse descended to the water level, as depicted in Figure 11d. After the earthquake, new cracks formed, existing tensional cracks widened, and the stone fillings along the coastal zone dropped towards the sea. Unlike the event on February 6, there was no observed sand ejecta at the ground surface.

Following the event on February 20, the coastal subsidence and lateral spreading of both the artificial fill and natural alluvium led to a new stage in the coastal area. For instance, the subsidence progressed to the point where seawater was able to pass the fishermen's port in front of İskenderun and enter the streets, as shown in Figure 11a. This occurred due to a combination of significant ground subsidence and rising sea levels caused by winds from the southwest. The streets were flooded again due to the earthquakes, but this time the water did come from the bay. Government agencies attributed this flooding event to the strong southwest winds. Before the event on February 20, there had been no history of a storm causing seawater to flood the streets.

After the harbor was submerged due to subsidence and lateral spreading, the structures in the coastal zone were exposed to tidal effects. There was a cyclical oscillation of seawater related to tides, resulting in rising in the evening and retreating in the morning. While the seawater entrance into the streets was primarily due to regional vertical and lateral movement of loose coastal sediments, officials linked this sea water emplacement to westward blowing winds.

Another aspect related to seawater intrusion was the dredging of mud to allow larger boats to enter the fisherman's harbor. However, this local sediment dredging activity cannot be the sole cause of the subsidence processes on a 1 km scale.

Figure 11b illustrates the widening of tension cracks. The lateral extension from the openings of five cracks on the wall, perpendicular to the shore, was measured as 34 cm (18 cm + 5 cm + 4 cm + 5 cm + 2 cm) over a 30 m dimension. This results in a lateral spread of around 1% from the combined movements of both the earthquakes on February 6 and February 20. In addition to the walls splitting/breaking, the surface water and wastewater collection channels that pass over the artificial fill zone and discharge into the sea were also damaged due to lateral extension.

Figure 11c shows how seawater intrusion into the park area caused the accumulation of gravel along the

Figure 9. Yellow arrows show lateral spreading cracks and circles indicate sand ejecta associated with the main earthquake.

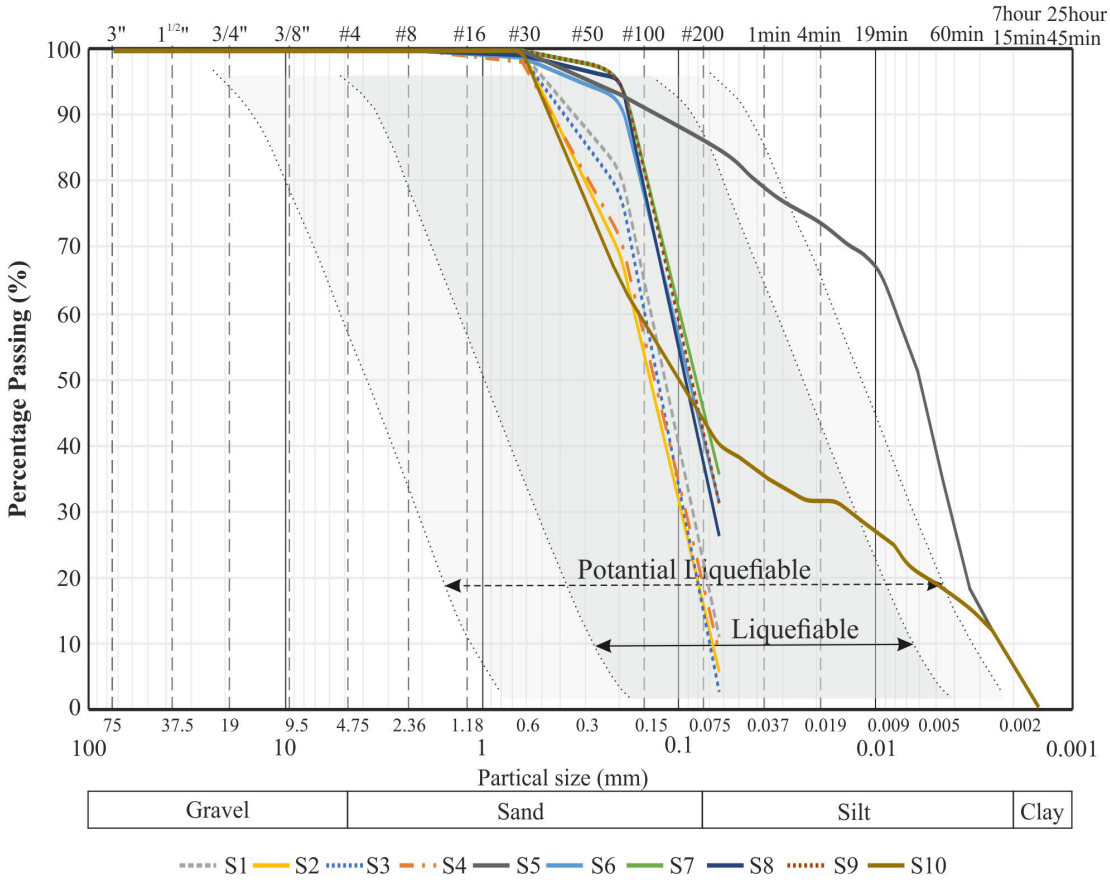

Figure 10. Granulometric analysis of the ten sand ejecta samples plotted on the Das (1983) diagram. The ejected materials primarily comprise fine-grained sand with 30 to 45 percent silt and clay. These size factions clearly fall within the liquefiable range.

grassy area. Due to the collapse of the coastal zone after the earthquake, waves piled up sea pebbles in the parks. Seawater infiltration along the opening cracks likely enhanced or triggered the lateral spreading and associated subsidence. After the earthquake on February 20, a cyclical or positive feedback mechanism led to subsidence-induced crack development and crack development-induced subsidence.

6. Discussion

Geological-geotechnical studies have indicated that the İskenderun coastal plain was shaped by the ongoing erosion of the front of the Amanos Mountains during the Quaternary period, subsequently filled with deltaic sediments comprising gravel, sand, silt, and mud (Aslaner, 1973; Özturk et al., 2021). In a settlement suitability study conducted by Denge Company in İskenderun, it was found that weak soils, saturated with water and exhibiting a risk of liquefaction, as well as low Standard Penetration Test (SPT) values, were prevalent throughout the entire settlement area (Denge, 2010).

According to the report from Denge Co., the coastal zone, which carries the risk of liquefaction, was filled in the 1980s. Land was reclaimed from the sea, and recreational areas were established along the coast (Figure 12). Subsequently, in the last 20 years, especially in specific areas, there has been a proliferation of dense structures exceeding 10 stories in height, constructed on the weak soil foundation of the coastal belt. Although we do not possess specific data, it is highly likely that there was regional settlement both before and after the earthquake on May 6, particularly concerning the construction of these tall buildings.

The concentration of settlement, flooding, and building collapses after the earthquakes on February 6, 2023, and February 20, 2023, in a particular area along the İskenderun coast, behind the Fisherman's port, suggests that soil liquefaction and subsequent settlement, which were more prominent in this area, are the main causes of the problems experienced in the wake of the earthquake.

Figure 11. Coastal zone photos after the February 20, 2023 earthquake: a) streets inundated by seawater due to a combination of eastward blowing winds and ground subsidence; b) widening of the opening cracks (please refer to the white wall) along the park or filling zone indicating lateral spreading at approximately 1 percent; c) sea water intrusion into the park area and accumulation of gravel along the green zone; d) settling of the lighthouse into the sea associated with the subsidence of the coastal zone after the earthquakes.

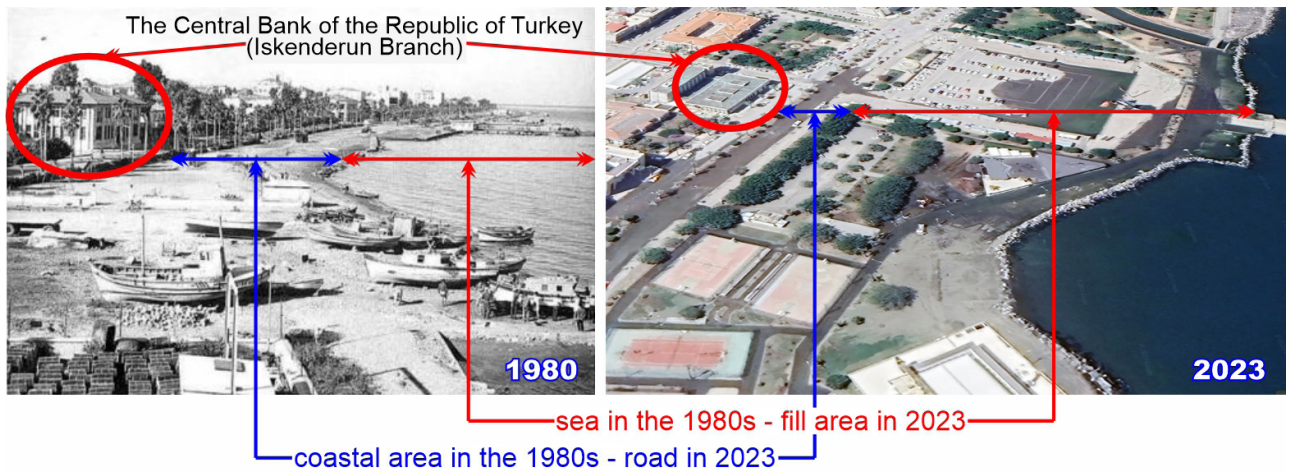

Figure 12. Changes in coastal, sea, and filling areas between 1980 and 2023.

The presence of similar ground conditions along the shores of İskenderun, coupled with observations of settlements, water inundation, and building damage in areas with dense multistory construction, underscores that the creation of high-rise buildings along the coast is the main reason for settlement and earthquake-induced disasters (Figures 13a–13c). Likewise, local settlement due to high-rise buildings beyond İskenderun, for instance, in the metropolitan area of Bursa in Türkiye, has been substantiated by lidar data (Aslan et al., 2019). The elevation of the shorter building situated between two multistory buildings indicates that the subsidence in İskenderun aligns closely with the height of the buildings.

Figure 13. a) Collapsed tall buildings along the İskenderun Bay due to the soil liquefaction, indicating weak soil conditions along the sea shore (Google Earth picture). b) Liquefaction-related sand ejecta from the soil along the buildings. c) Relatively low subsidence area between two subsided tall buildings along the İskenderun coastal zone.

Figure 14 illustrates the ground settlement pattern, lateral spreading, groundwater and sand spouts, as well as streets filled with water and sand, observed on the shores of İskenderun after the earthquakes of February 6, 2023, and February 20, 2023. Sand dikes and sand cones related to soil liquefaction during and after the earthquake are illustrated in Figures 14a–14d). They are observed in both natural alluvium and areas with relatively thin artificial fill. The presence of opening joints and sand outlets, roughly parallel to the shore, provides clear evidence of seaward spreading. Coastal lighthouses or fishing port facilities were used as reference points for regional subsidence. Following the earthquake on February 6, 2023, the surface rupture passed 20 m east of the İskenderun settlement. According to these reference points, the shores of İskenderun subsided by 0.8 m. Subsequently, due to ongoing aftershocks and the 6.4 magnitude earthquake that occurred 22 km east of the settlement on February 20, 2023, the subsidence accelerated, resulting in a total settlement of 1.7 m (Figures 14e–14f). In the case of lateral spreading, the extent of tension cracking was measured and its percentage was calculated. Particularly, based on the observed opening cracks in the walls perpendicular to the shore, it was determined that the lateral spread, which was 0.6 percent on February 2, increased to one percent on February 20. This serves as compelling evidence of the expansion towards the sea along the coasts. The settlement observed in İskenderun's coastal areas, along with the encroachment

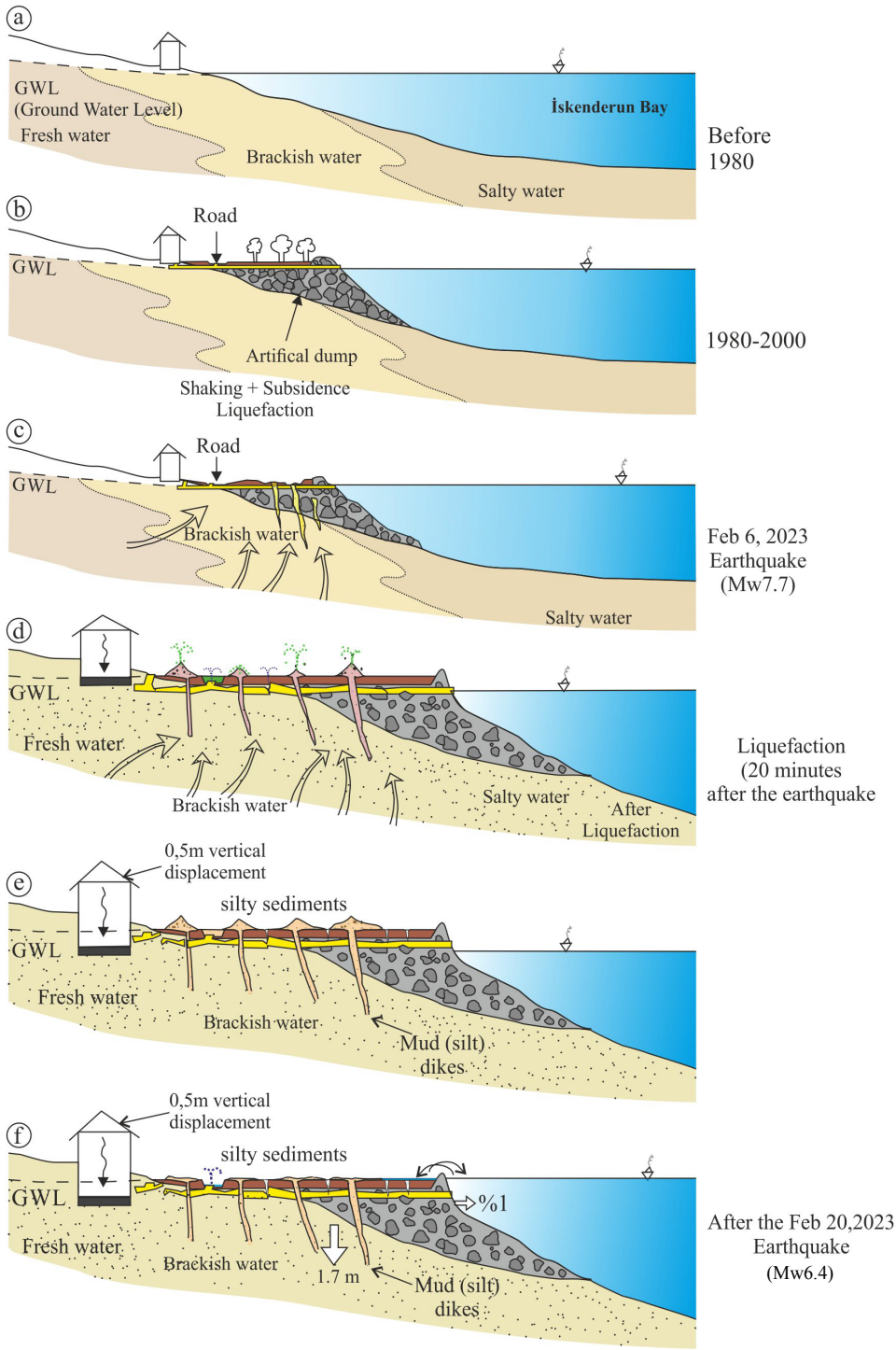

Figure 14. a) Model depicting the development of the İskenderun coastal zone before the 1980s. b) Filling of the coastal zone extending up to 2 km in length and 200 m in width. c) Shaking and formation of sand ejecta associated with liquefaction water during the major earthquake on February 6, 2023 (Mw 7.7). The water originated from liquefaction and a broken sewage or water supply system, which flooded the streets (marked in green) after the earthquake and remained for five days before being pumped into the sea. Some buildings settled by about 0.5 m, tilted, or failed due to liquefaction in close proximity to the coastal zone. Coastal subsidence and lateral spreading were intensified, and seawater began to invade the green zone and fisherman port after the February 20, 2023 earthquake (Mw: 6.4).

of seawater, may have been experienced by ancient cities in the past. Instances like Alexandria and the submerged cities off the coast of Egypt (Mostafa et al., 2000; Abd-el-Maguid, 2012; Nemo, 2022) further demonstrate that weak delta sediments, possibly related to earthquakes, may have undergone lateral spreading due to seismic events in the past, resulting in collapses similar to what occurred in İskenderun.

7. Conclusion

On the shores of İskenderun, after the Mw 7.7 Pazarcık earthquake on February 6, 2023, possibly the largest soil liquefaction event in Türkiye occurred. Soil liquefaction took place both in the natural alluvial ground along the coast and in the filled areas near the seashores.

Following the earthquake, brackish (partly salty) water under the artificial coastal fill also carried fine sands from its base and erupted onto the surface. The fine sands from the groundwater, bursting out from hundreds of points, flooded the roads. After the liquefaction stopped, water boiled up from beneath the ground, leaving behind pools of water and hundreds of tons of sand in the streets and green areas along the coast. The earthquake also led to the destruction of the sewage and water supply system, contributing to the flooding of the streets.

As reported by the national media, after the initial major earthquake, seawater did not flood the shores, nor did it seep in from the shores. The water that emerged from below was brackish and formed from the mixture of groundwater and lagoon water. However, subsidence continued after the main earthquake and was triggered by the earthquake on February 20, 2023, resulting in a 1.7-m subsidence. Following this event, seawater began to inundate the green zone due to the influence of waves and tides.

The lighthouse, which serves as a fixed reference point, has settled by approximately 1.7 m and is still undergoing further settling. These ongoing processes provide a valuable opportunity for comparing subsidence in ancient cities related to regional liquefaction. The most significant indicators of soil liquefaction in buildings include the tilting of many tall buildings and the shifting of their axes. Given the liquefaction potential of the geological environment, decision makers should exercise caution when considering development in coastal plains.

Acknowledgment

This study was partially supported by TÜBİTAK-MAM 1002-c project titled "The Fault Parameters of the Earthquakes Dated February 06, 2023 and the Investigation of the Effects in the Region". We would also like to extend our thanks to the Turkish Research Foundation for their logistical support, and to the Turkish Army officials for providing us with video recordings.

References

Abd-el -Maguid MM (2012). Underwater archaeology in Egypt and the protection of its underwater cultural heritage. Journal of Maritime Archaeology 7 (1): 193-207.

AFAD (2023). 06 Şubat 2023 Pazarcık (Kahramanmaraş) Mw 7.7 Elbistan (Kahramanmaraş) Mw 7.6 Depremlerine İlişkin Ön Değerlendirme Raporu. Ankara: T.C. İçişleri Bakanlığı Afet ve Acil Durum Yönetimi Başkanlığı Deprem ve Risk Azaltma Genel Müdürlüğü Deprem Dairesi Başkanlığı (in Turkish).

Andrus RD, Arango I, Castro G, Christian JT, Dobry R et al. (2001). Liquefaction resistance of soils: summary report from the 1996 NCEER and 1998 NCEER/NSF workshops on evaluation of liquefaction resistance of soils. Journal of Geotechnical and Geoenvironmental Engineering 127 (10).

Arel E, Önalp A (2012). Geotechnical properties of Adapazari silt. Bulletin of Engineering Geology and the Environment 71 (4): 709-720.

Aslan G, Çakir Z, Lasserre C, Renard F (2019). Investigating subsidence in the Bursa Plain, Turkey, using ascending and descending Sentinel-1 Satellite data. Remote Sensing 2019; 11 (1): 85. https://doi.org/10.3390/rs11010085

Aslaner M (1973). İskenderun-Kırıkhan bölgesindeki ofiyolitlerin jeoloji ve petrografisi. MTA Publ., 150: 78, Ankara (in Turkish).

Bray JD, Macedo J (2017). 6th Ishihara lecture: Simplified procedure for estimating liquefaction induced building settlement. Soil Dynamics and Earthquake Engineering, 102: 215-231.

Das BM (1983). Fundamental of Soil Dynamics, Elsevier Science Publishing Co. Inc., Amsterdam, the Netherlands.

Davis CA, Giovinazzi S, Hart DE (2015), "Liquefaction Induced Flooding in Christchurch, New Zealand," 6th Int. Conf. on Earthquake Geotechnical Engineering, Christchurch, NZ, International Society on Soil Mechanics and Geotechnical Engineering, Nov. 1-4.

Denge Engineering Co. (2010). Hatay İli, İskenderun İlçesi, İskenderun Belediyesi, Mikrobölgeleme Etüd Raporu, Hatay (in Turkish).

Dixon TH, Amelung F, Feretti A, Novali F, Rocca F et al. (2006). Subsidence and flooding in New Orleans. Nature 441: 587-588. https://doi.org/10.1038/ 441587a.

Galavi, V, Petalas A, Brinkgreve R (2013). Finite element modelling of seismic liquefaction in soils. Geotechnical Engineering Journal of the SEAGS & AGSSEA 44 (3): 55-64.

Green RA, Cubrinovski M, Cox B, Wood C, Wotherspoon L et al. (2014). Select liquefaction case histories from the 2010–2011 Canterbury Earthquake Sequence. Earthquake Spectra, 30: 131– 153. https://doi.org/10.1193/030713EQS066M.

Giovinazzi S, Wilson TM, Davis CA, Bristow D, Gallagher M et al. (2011). Lifelines performance and management following the 22 February 2011 Christchurch earthquake, New Zealand: highlights of resilience. http://hdl.handle.net/10092/6358.

Goldberg DE, Taymaz T, Reitman NG, Hatem AE, Yolsal Çevikbilen Y et al. (2023) Rapid Characterization of the February 2023 Kahramanmaraş, Türkiye, Earthquake Sequence. The Seismic Record 2023; 3 (2): 156-167. https://doi.org/10.1785/0320230009

Hidayat RF, Kiyota T, Tada N, Hayakawa J, Nawir H (2020). Reconnaissance on liquefaction-induced flow failure caused by the 2018 Mw 7.5 Sulawesi earthquake, Palu, Indonesia. Journal of Engineering and Technological Sciences 52 (1): 51-65.

Ishihara K, Yoshimine M (1992). Evaluation of settlements in sand deposits following liquefaction during earthquake. Soils and Foundations 32 (1): 173-188.

Lemke RW (1967). Effects of the earthquake of March 27, 1964, at Seward, Alaska: U.S. Geological Survey Professional Paper 542–E: 43 p. https://pubs.usgs.gov/pp/0542e/.

Mase LZ, Tanapalungkorn W, Likitlersuang S, Ueda K, Tobita T (2022). Liquefaction analysis of Izumio sands under variation of ground motions during strong earthquake in Osaka, Japan. Soils and Foundations 62 (5): 101218.

Measures RJ, Hicks DM, Shankar U, Bind J, Arnold J et al. (2011). Mapping earthquake induced topographical change and liquefaction in the Avon-Heathcote Estuary. NIWA Client Report CHC2011-066, Prepared for Environment Canterbury, 28 p.

Mostafa MH, Grimal N, Nakashima D (2000). Underwater Archaeology and Coastal Management: Focus on Alexandria. Paris, France: UNESCO. Retrieved from http://unesdoc.unesco.org/images/0011/001197/119751eb.pdf

Nemo L (2022) Stop Searching for Atlantis and Find These 4 Ancient Underwater Cities Instead, Discover, https://www.discovermagazine.com/planet-earth/forget-atlantis-heres-4-real-ancient-underwater-cities.

Öztürk H, Hanilci N, Cansu Z., Kasapci C (2021). Formation of Ti-rich bauxite from alkali basalt in continental margin carbonates, Payas region, SE Turkey: implications for sea level change in the Upper Cretaceous. Turkish Journal of Earth Sciences 30 (1): 116-141.

Quigley MC, Bastin S, Bradley BA (2013). Recurrent liquefaction in Christchurch, New Zealand, during the Canterbury earthquake sequence: Geology 41: 419-422, https://doi.org/10.1130/G33944.1.

Quintero J, Saldanha S, Millen M, Viana da Fonseca A, Sargin S et al. (2018). Investigation into the Settlement of a Case Study Building on Liquefiable Soil in Adapazari, Turkey. 5th Geotechnical Earthquake Engineering and Soil Dynamics Conference: Liquefaction Triggering, Consequences, and Mitigation, GEESDV 2018: 321-336. Texas, United States of America.

Seed HB, Idriss IM (1971). Simplified Procedure for Evaluating Soil Liquefaction Potential. Journal of the Soil Mechanics and Foundations Division, ASCE 97 (9): 1249-1273.

Seed, HB, Cetin KO, Moss RES, Kammerer AM, Wu J et al. (2003). Recent advances in soil liquefaction engineering: A unified consistent framework. Berkeley, California: Earthquake Engineering Research Institute.

Tanaka Y (1996). Liquefaction of reclaimed lands along Osaka Bay by great Hanshin earthquake (1995.1. 17). In The Sixth International Offshore and Polar Engineering Conference 1: 20-28.

Villamor P, Almond P, Tuttle MP, Giona Bucci M, Langridge RM et al. (2016). Liquefaction Features Produced by the 2010–2011 Canterbury Earthquake Sequence in Southwest Christchurch, New Zealand, and Preliminary Assessment of Paleoliquefaction Features. Bulletin of the Seismological Society of America 106 (4): 1747-1771. https://doi.org/10.1785/0120150223